THE JOURNAL OF PHYSICAL CHEMISTRY LETTERS
A JOURNAL OF THE AMERICAN CHEMICAL SOCIETY

pubs.acs.org/JPCL

Letter

# Breaking the Symmetry of Pyrimidine: Solvent Effects and Core-Excited State Dynamics

Sebastian Eckert,* Vinícius Vaz da Cruz,* Miguel Ochmann, Inga von Ahnen, Alexander Föhlisch, and Nils Huse

Cite This: *J. Phys. Chem. Lett.* 2021, 12, 8637−8643

Read Online

ACCESS | Metrics & More | Article Recommendations | Supporting Information

**ABSTRACT:** Symmetry and its breaking crucially define the chemical properties of molecules and their functionality. Resonant inelastic X-ray scattering is a local electronic structure probe reporting on molecular symmetry and its dynamical breaking within the femtosecond scattering duration. Here, we study pyrimidine, a system from the $C_{2v}$ point group, in an aqueous solution environment, using scattering though its $2a_2$ resonance. Despite the absence of clean parity selection rules for decay transitions from in-plane orbitals, scattering channels including decay from the $7b_2$ and $11a_1$ orbitals with nitrogen lone pair character are a direct probe for molecular symmetry. Computed spectra of explicitly solvated molecules sampled from a molecular dynamics simulation are combined with the results of a quantum dynamical description of the X-ray scattering process. We observe dominant signatures of core-excited Jahn−Teller induced symmetry breaking for resonant excitation. Solvent contributions are separable by shortening of the effective scattering duration through excitation energy detuning.

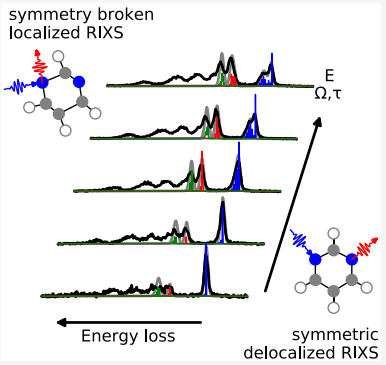


According to the Jahn−Teller theorem, degeneracy of electronic states of a molecule is lifted through symmetry reductions, yielding a total energy minimization. This symmetry breaking is mediated by vibronic coupling between the electronic states via antisymmetric vibrational modes.[1] This effect is of particular importance for core-excited electronic states, as a multitude of near-degenerate core-levels are present for identical atoms in symmetric molecules.[2] The initially delocalized core-orbitals dynamically localize in the symmetry-broken configurations within the core-hole lifetime.[3−6] Resonant inelastic X-ray scattering (RIXS), also called resonant X-ray Raman scattering, is capable of addressing this dynamical localization problem via the excitation energy dependence of the spectral profile, based on the concept of the effective scattering duration.[7] Violations of quadrupole selection rules in soft X-ray RIXS, i.e., resonant enhancement of symmetry forbidden transitions, have proven to sensibly detect Jahn−Teller induced symmetry breaking in core-excited states for linear triatomic molecules in the gas phase[5,8] and for larger organic systems.[9,10] Recently, RIXS has evolved as a powerful tool to access the electronic structure of molecules in solution, for studies of, e.g., proton dynamics[11−13] and transition metal complexes.[14−16] These fluctuating environments[17] can induce geometric distortions in the electronic ground state independent of the X-ray excitation. Therefore, the competition of solvent-induced symmetry breaking and Jahn−Teller distortions in the core-excited state needs to be considered for quantitative understanding of RIXS measurements of symmetric systems.

Many recent studies utilizing RIXS have targeted nitrogen-conjugated heterocycles as fundamental building blocks of larger biomolecules[18−20] and as ligands in metal-complexes[21] used for catalysis and energy harvesting.[22] In this context, we report on a quantitative combined experimental and theoretical investigation of the RIXS spectra of aqueous pyrimidine, as a prime example of the interplay between the two symmetry breaking mechanisms. Pyrimidine belongs to the $C_{2v}$ point group, containing two identical nitrogens, which are acceptors of strong solute−solvent hydrogen bonds,[23−26] via their in plane lone-pair orbitals. These hydrogen bonding orbitals are directly probed in nitrogen K-edge RIXS through their local 2p character.

RIXS is a coherent scattering process, where the investigated system is promoted to a set of core-excited states, followed by decay onto the manifold of valence excited states.[6] Here, we focus on resonant scattering via the lowest unoccupied molecular orbital (LUMO) of pyrimidine, namely through a transition from the N 1s orbitals to the antibonding orbital $2a_2$, with N−C $\pi^*$ character changing sign across the reflection plane $\sigma_v(xz)$, between the nitrogen atoms of pyrimidine. The intense absorption line corresponding to this transition, which

**Received:** June 11, 2021
**Accepted:** August 3, 2021
**Published:** September 2, 2021

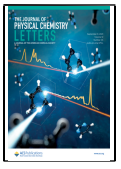





https://doi.org/10.1021/acs.jpclett.1c01865
*J. Phys. Chem. Lett.* 2021, 12, 8637−8643

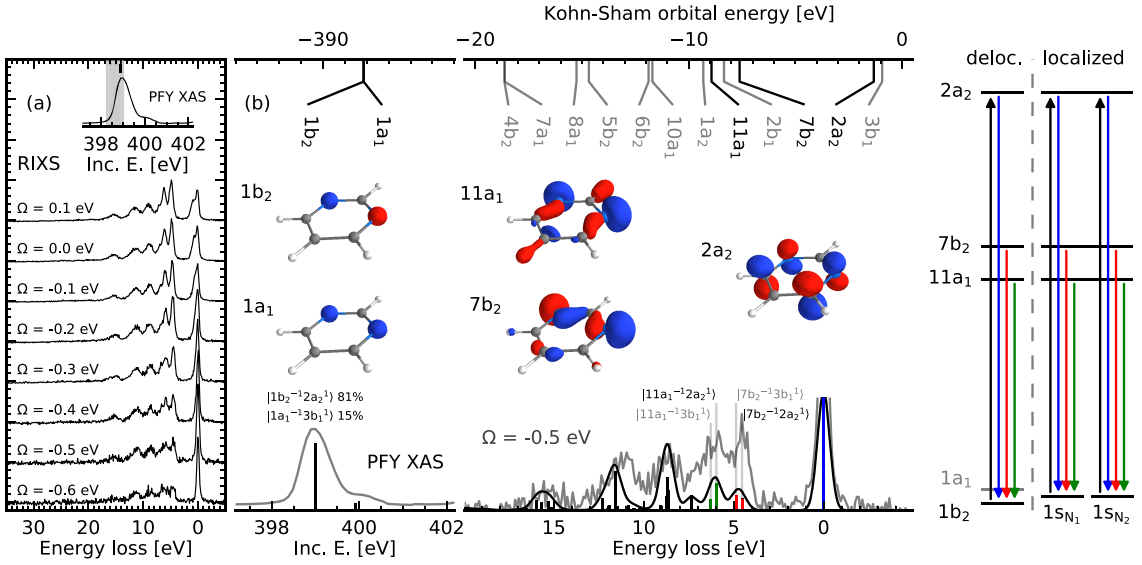


**Figure 1.** RIXS at the nitrogen K-edge $\pi^*$-resonance of aqueous pyrimidine. The two energetically lowest inelastic emission channels in the experimental spectra (a) exhibit a strongly detuning-dependent intensity. Theoretical simulations of the electronic structure an the transition amplitudes (b) of pyrimidine in a fully symmetric geometry allow for an assignment of the detuning dependent emission lines to decay from the $7b_2$ and $11a_1$ orbitals, subsequent to excitation into the $2a_2$ orbital. The experimental spectra are shown in gray.

**Table 1. Transition Dipole Moments (in Atomic Units $e \times a_0$) between the RSA-TD-DFT States Involved in the RIXS Process Assigned According to the Largest One-Electron Transition Character**

| delocalized/adiabatic picture | | | | localized/diabatic picture | | | |
|---|---|---|---|---|---|---|---|
| transition | $\mu^x$ | $\mu^y$ | $\mu^z$ | transition | $\mu^x$ | $\mu^y$ | $\mu^z$ |
| $1a_1 \rightarrow 2a_2$ | 0.0000 | 0.0000 | 0.0000 | $1s_{N_1} \rightarrow 2a_2$ | 0.0000 | 0.0000 | −0.0586 |
| $1b_2 \rightarrow 2a_2$ | 0.0000 | 0.0000 | −0.0828 | $1s_{N_2} \rightarrow 2a_2$ | 0.0000 | 0.0000 | 0.0586 |
| $7b_2 \rightarrow 1a_1$ | 0.0000 | 0.0505 | 0.0000 | $7b_2 \rightarrow 1s_{N_1}$ | 0.0125 | 0.0354 | 0.0000 |
| $7b_2 \rightarrow 1b_2$ | 0.0179 | 0.0000 | 0.0000 | $7b_2 \rightarrow 1s_{N_2}$ | −0.0125 | 0.0354 | 0.0000 |
| $11a_1 \rightarrow 1a_1$ | −0.0405 | 0.0000 | 0.0000 | $11a_1 \rightarrow 1s_{N_1}$ | −0.0283 | −0.0196 | 0.0000 |
| $11a_1 \rightarrow 1b_2$ | 0.0000 | −0.0279 | 0.0000 | $11a_1 \rightarrow 1s_{N_2}$ | −0.0283 | 0.0196 | 0.0000 |

is energetically well separated from the onset of the continuum absorption, is shown in Figure 1a. In the delocalized picture, due to $C_{2v}$ symmetry, the antisymmetric $1b_2$ and the symmetric $1a_1$ core-orbitals exist as linear combinations of the degenerate nitrogen 1s orbitals. In this framework the transition to the $|1a_1^{-1}2a_2^{1}\rangle$ is symmetry forbidden, as the contributions to the transition dipole at the two nitrogen sites are inversely oriented and thus cancel, as expected by the $C_{2v}$ dipole selection rules (see Table 1). Thus, in the symmetric ground-state configuration only transitions from the symmetry adapted $1b_2$ core-orbital contribute to the absorption intensity. Note that the minor CI admixture of the $|1a_1^{-1}3b_1^{1}\rangle$ excitation to the $\pi^*$-resonance will be neglected in our discussion.

In the coupled emission step, decay from the occupied bonding orbitals with large N 2p character are observed in the range of 0−20 eV. The most prominent signatures at resonant excitation are the two intense and narrow emission lines at approximately 5 and 6 eV energy loss. To assess the origin of the different emission features, we focus on the electronic structure and RSA-TD-DFT[27] spectrum simulations (based on the Kramers−Heisenberg formalism) of the fully symmetric isolated pyrimidine molecule in Figure 1b. Thereby, we relate the emission lines to decay from the symmetric and antisymmetric combination of occupied lone-pair orbitals, the $11a_1$ and $7b_2$ orbitals (see Figure 1b), these orbitals are split by ∼1 eV due to overlap with the ring $\sigma$ orbitals. The calculated spectrum does not reproduce the experimental spectrum for resonant excitation $\Omega = 0$ eV, where $\Omega$ is the detuning defined as $\Omega = \omega - \omega_{res}$, where $\omega$ and $\omega_{res}$ are the incoming photon energy and the energy of resonant absorption, respectively. The low predicted intensity can be understood by examining the lone-pair orbitals. Despite the absence of clean selection rules for the $7b_2$ and $11a_1$ orbitals, they point at a wide angle with respect to the symmetry axis, leading to a substantial cancellation of the largest component of the transition dipole moments for emission and resulting in an effective quenching of the intensity, even-though these orbitals are largely concentrated on the nitrogen atoms (see Table 1). The experimental data shows a gradual decrease of the lone pair scattering intensity with the detuning $\Omega$, yielding an improved agreement with the computed spectrum at $\Omega = -0.5$ eV, as shown in direct comparison in Figure 1b.

The underestimation of the peak intensities for the $7b_2$ and $11a_1$ emission lines in the simulations indicates the presence of symmetry-broken molecular configurations under the experimental conditions. Deviation from the fully symmetric chemical environment of the two nitrogen sites lifts the degeneracy of the nitrogen 1s orbitals, causing a localization of the core-holes. The localized scattering picture is generally equivalent to the delocalized one when interference between


https://doi.org/10.1021/acs.jpclett.1c01865
J. Phys. Chem. Lett. 2021, 12, 8637−8643

the degenerate channels is considered.[3] However, the interference term can be quenched in solution due to the fluctuation of the environment. The same term can also be affected by nuclear dynamics, via the Jahn−Teller effect. In this case, the two localized states couple via an antisymmetric vibration within the short nitrogen core-hole lifetime. Both mechanisms induce a loss of coherence between the emission from the two nitrogen sites, leading to an amplification of the scattering intensity. Pyrimidine has both, two near-degenerate core-excited states as well as the ability to form hydrogen bonds with the solvent. Thus, both mechanisms must be investigated as the source of the observed drastic intensity enhancement upon resonant excitation.

We formulate the described problem in a more quantitative manner. Assuming the localized picture, the two core-excited states are defined as $|k\rangle \equiv |1s_{N_k}^{-1}2a_2^1\rangle$ with $k \in \{1, 2\}$. In this picture, the RIXS cross-section $\sigma_f(\omega', \omega)$ is proportional to the square of the scattering amplitude $F_{f,\nu_f}$ written as a sum of the two channels

$$F_{f,\nu_f} = F_{f,\nu_f}^{(1)} + F_{f,\nu_f}^{(2)} \tag{1}$$

Due to the symmetry breaking in the intermediate state we must consider the nuclear degrees of freedom to correctly describe the problem. Assuming the Born−Oppenheimer and Franck−Condon approximations, we introduce the electronic transition dipole moments $\mu_{nm} = \langle n|\mathbf{r}|m\rangle$ between the $m$th and $n$th electronic states. Within these assumptions, we write the Kramers−Heisenberg scattering amplitude

$$F_{f,\nu_f}^{(k)} = -\mathrm{i}(\mathbf{e}'\cdot\boldsymbol{\mu}_{fk})(\mathbf{e}\cdot\boldsymbol{\mu}_{k0}) \times \langle \nu_f|\Psi_k(\omega)\rangle \tag{2}$$

where $\mathbf{e}$ and $\mathbf{e}'$ are the incoming and outgoing photon polarization vectors, respectively. The core-excited wave packet[17,28] $|\Psi_k(\omega)\rangle$ describes vibrational interference effects and the nontrivial dependence on the incoming photon energy

$$|\Psi_k(\omega)\rangle = \mathrm{i}\sum_{\nu_k} \frac{|\nu_k\rangle\langle\nu_k|\nu_0\rangle}{\omega - \omega_{k0} - (\epsilon_{\nu_k} - \epsilon_{\nu_0}) + \mathrm{i}\Gamma} \tag{3}$$

To assess the impact of the fluctuating solvent network on the symmetry of the two nitrogen sites in pyrimidine, we carried out molecular dynamics (MD) simulations. In this case, we momentarily ignore the role of quantum vibrations, by making the following replacements $F_{f,\nu_f} \rightarrow F_f$ and $\langle \nu_f|\Psi_k(\omega)\rangle \rightarrow \mathrm{i}/(\omega - \omega_{k0} + \mathrm{i}\Gamma)$ in the equations above.

We analyze the results of the MD simulation with respect to geometric distortions induced by coordination with the surrounding water molecules. Pyrimidine accepts one hydrogen bond (HB) per nitrogen atom, the donated hydrogen atoms from water point inward and are distributed symmetrically across the ring plane. This result is in agreement with earlier studies.[25,29] The effect of the HBs is shown by the solvent densities in Figure 2a. At the same time, the distortions induced by the thermal motion as well as solvent fluctuations can be estimated by the overlay of $10^4$ geometry snapshots. It reveals that the ring structure experiences only small fluctuations. The main effect of solvation on the C−N bonds of the ring is to elongate them, with respect to the optimized geometry, as shown by the 2D histogram in Figure 2b. Otherwise, a fully symmetric histogram of the bond lengths between the nitrogen sites and the connecting carbon $d_{C-N_{1/2}}$ is observed as a result of the rigidity and planarity of pyrimidine's

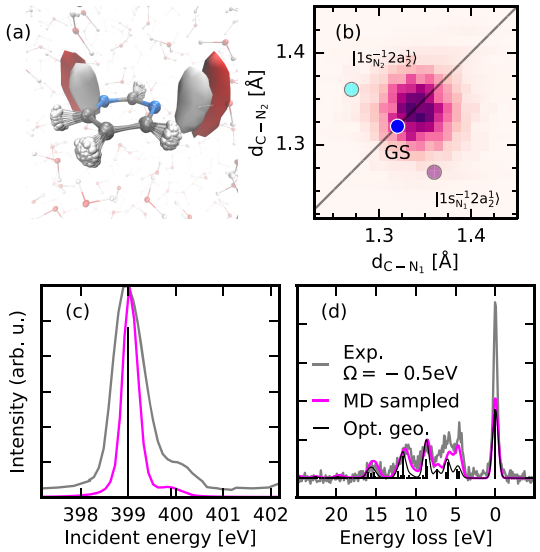


**Figure 2.** Solvent-induced symmetry breaking from MD-sampling. The overlay of $10^4$ structures with solvent densities (a) as well as the histogram of the N−C bond lengths (b) reflect the rigidity of the pyrimidine ring in aqueous solutions. The bond lengths for the optimized structures in the electronic ground and nitrogen 1s core-excited states are shown. Solvent induced broadening and shift of the $\pi^*$ absorption resonance (c) with respect to the simulation in the optimized molecular geometry. The intensity of the $7b_2$ and $11a_1$ transitions in the resonant MD-sampled RIXS spectrum agree well with the intensity detected in the detuned experimental spectrum (d).

aromatic ring.[29,30] To understand the impact of the solvent environment on the X-ray spectra, 200 uncorrelated snapshots have been sampled to compute an averaged absorption spectrum in Figure 2c and the RIXS spectrum in Figure 2d. To account for covalent intermolecular interactions, all water molecules within the first solvation shell around the nitrogen atoms of pyrimidine were explicitly included in the spectrum simulations.

The shape of the X-ray absorption spectrum is well captured. Comparison to the simulation for the optimized molecular structure shows that the solvent environment merely induces a broadening of the $\pi^*$ absorption resonance. Additionally, a shift on the order of 0.1 eV toward higher photon energies, which is a general trend for deprotonated nitrogen atoms in conjugated heterocycles.[31,32] In contrast, the effect of the sampling on the RIXS spectrum is significant, as the previously discussed interference between nitrogen sites is suppressed, enhancing the intensity for decay from the $11a_1$ and $7b_2$ orbitals in the nonsymmetric solvent environment. Even though only minor deviations from the $C_{2v}$ symmetry occur, a significant increase of the two lone-pair transitions compared to the optimized symmetric molecular structure is observed. The strong impact of the solvent on these transitions directly reflects the hydrogen bonding character of the involved orbitals.

The simulated RIXS spectrum including solvent interactions, however, does not reproduce the experimental intensities of the lone-pair peaks for resonant excitation. In spite of that, the detuned experimental spectrum and the resonant theoretical sampled spectrum are in excellent agreement. At a detuning of $\Omega = -0.5$ eV the effects of core-excited state dynamics are diminished as scattering can be regarded as instantaneous under largely detuned conditions.[7] Hence, only the spectral


https://doi.org/10.1021/acs.jpclett.1c01865
J. Phys. Chem. Lett. 2021, 12, 8637−8643

signatures of solvent fluctuations remain, which are not quenched by excitation energy detuning.

Not only the intensity increase of the lone-pair emission lines for resonant excitation (Ω = 0 eV), but also the pronounced asymmetry of the elastic line (due to the vibrational progression extending from 0 to 2 eV energy loss) are strong indications for symmetry breaking through ultrafast dynamics within the scattering duration. The comparison to the detuned spectrum in Figure 2d shows, that the neglect of core-excited state dynamics in the MD-sampled spectrum simulation results in a poor agreement for the relative intensities of the electronically elastic and inelastic scattering channels. The extent of core-excitation induced symmetry breaking can be estimated from the optimized geometries in the $|1s_{N_k}^{-1}2a_2^{1}\rangle$ states. The position of the minima for the C−N bonds are marked in Figure 2b. As expected by the Jahn−Teller effect, the two near degenerate core-excited states are split into two opposite minima, along a mostly antisymmetric reaction coordinate.

Now, we turn to the full vibronic Kramers−Heisenberg treatment of eq 3. We do so by constructing a reduced dynamical model, including a normal-mode analysis combined with core-excited potential energy scans, considering only implicit solvation (see Supporting Information). We determined that the 8a ($a_1$) and 8b ($b_2$) pair of near-degenerate stretching modes[33] of pyrimidine are the most active in the RIXS process. We construct the total vibrational wave function for electronic state $k$ as $|\nu_k\rangle = |\nu_k^{(s)}\rangle|\nu_k^{(a)}\rangle$ and energies as $\epsilon_{\nu_k} = \epsilon_{\nu_k^{(s)}} + \epsilon_{\nu_k^{(a)}}$. In the equations above, we label 8b as (a) and 8a as (s). Note that only antisymmetric stretching modes can mediate the symmetry breaking. Still, the inclusion of the symmetric stretching mode in the spectrum simulations is essential for a correct description of the vibrational profile of the absorption spectrum and the resulting detuning dependent RIXS spectra. The core-excited state potential energy surfaces along the 8b mode, presented in Figure 3a, show the expected Jahn−Teller effect, lifting the degeneracy of the $|1b_2^{-1}2a_2^{1}\rangle$ and $|1a_1^{-1}2a_2^{1}\rangle$ states. This imposes forces on the core-excited molecule at the vertical point, which drives the nuclear wavepackets of the two states in opposite directions for Ω = 0.0 eV. The further the wave packets move apart, the larger the symmetry breaking effect. Strictly, the degree of electronic interference in the scattering is directly proportional to the overlap between the two core-excited wave packets (see Supporting Information for a mathematical proof). Indeed, we can define a symmetry breaking parameter as

$$\zeta(\omega) = 1 - \mathrm{Re}\frac{\langle\Psi_1(\omega)|\Psi_2(\omega)\rangle}{\langle\Psi_1(\omega)|\Psi_1(\omega)\rangle} \tag{4}$$

for which symmetry breaking is maximum for $\zeta = 1$, while being absent for $\zeta = 0$. Next, we analyze the effect of detuning. For resonant excitation, scattering occurs from largely distorted geometries along $Q_a$ yielding a small overlap between the wave packets $\langle\Psi_1|\Psi_2\rangle \ll \langle\Psi_1|\Psi_1\rangle \Rightarrow \zeta \approx 1$. In this limit, the core-holes are effectively localized and the enhancement of the lone-pair emission results mainly from the reduction of the scattering cross-section to the incoherent sum of scattering through the individual core-states. In contrast, for a detuning of Ω = −0.6 eV the spectral signatures of symmetry breaking are suppressed, because $\langle\Psi_1|\Psi_2\rangle \approx \langle\Psi_1|\Psi_1\rangle \Rightarrow \zeta \approx 0$ (see Figure 3a) yielding the ground-state electronic RIXS spectrum, dressed by vibrational fine-structure. In this limit, we recover

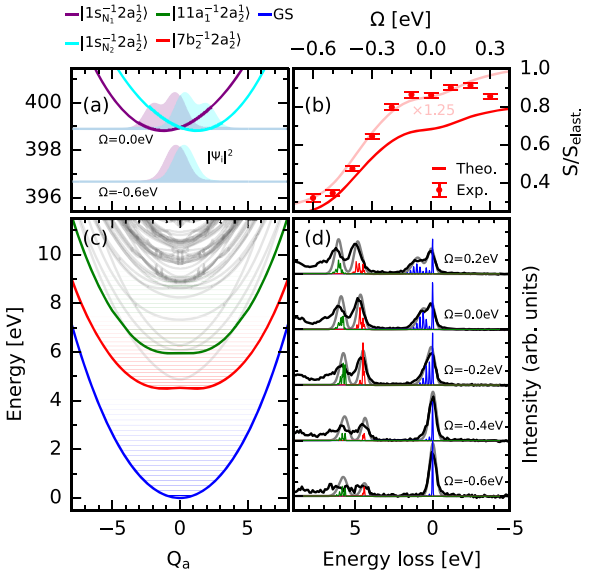


**Figure 3.** Symmetry breaking induced by core-excitation. Core (a) and valence excited state potentials together with the ground state potential (c) along the antisymmetric stretching coordinate ($Q_a$). The detuning dependent degree of symmetry breaking in the core-excited state is reflected in the respective wavepackets in part a. This drastically affects the intensity ratio between the $|11a_1^{-1}2a_2^{1}\rangle$ and the electronically elastic scattering channel (b) and induces different vibrational substructures of the individual spectral lines (d, colored). In part d the sum of the individual electronic channels (gray, 0.4 eV fwhm Gaussian broadening) is compared to the experimental data (black).

the previously discussed partial cancellation of the transition dipole moments and closing of the $1a_1$ scattering channel. The electronically elastic scattering channel exhibits opposite behavior, namely an intensity quenching for resonant excitation.

Further information can be extracted from analyzing the spectral profile of the individual electronic final states. In Figure 3d, we compare simulated and experimental RIXS spectra as a function of detuning. Overall both peak shapes and relative intensities resulting from the dynamical simulations are in excellent agreement with the experimental detuning dependent spectra. As can be seen directly from the scattering intensity of the electronically elastic transitions (Figure 3d, blue), population of high-lying vibrational levels as RIXS final states directly reflect the detuning-dependent amplitude of the core-excited state wave packet projected onto the comparably steep ground state potential energy curve.[34] In contrast to the electronically elastic transitions, the shallowness of the valence excited state potentials in Figure 3c results in a reduced separation of the vibrational levels as well as wider expansion of vibrational wave functions. The low spacing of the levels results in very narrow vibrational profiles for the $|11a_1^{-1}2a_2^{1}\rangle$ (red) and $|7b_2^{-1}2a_2^{1}\rangle$ (green) presented in Figure 3d.

The effects described are nicely summarized in the detuning dependent ratio between the integral RIXS cross sections for scattering into the $|7b_2^{-1}2a_2^{1}\rangle$ and the electronic ground-state (decay from the same excited $2a_2$ orbital) in Figure 3b. The presented ratios result from the integrals of the vibrationally resolved cross sections for the individual final states presented in Figure 3d. The experimental values result from areas of Gaussian line profiles fitted to the spectra. The simulated ratios


https://doi.org/10.1021/acs.jpclett.1c01865
J. Phys. Chem. Lett. 2021, 12, 8637−8643

model the detected drastic increase of the lone-pair emission with respect to the elastic scattering. The simulations underestimate the total amplitude of the ratio by roughly a factor of 1.25. This can result from effects of hydrogen bonding and solvent induced symmetry breaking, discussed in the context of Figure 2, which are neglected in the presented quantum dynamical model.

In summary, the pyrimidine molecule, belonging to the $C_{2v}$ point group, serves as a showcase for transition dipole moment cancellation in resonant inelastic X-ray scattering. The drastically reduced intensity for radiative decay channels from nitrogen-centered lone pair orbitals $7b_2$ and $11a_1$ within their symmetric ground state geometry underscores the importance of symmetrized orbitals that underlie these cancellation mechanisms. This propensity is violated for resonant excitation where very intense emission lines are restored due to Jahn−Teller-induced nuclear dynamics in the excited state that lead to a reduction in molecular symmetry. Shortening the scattering time by detuning from resonance suppresses the nuclear dynamics but does not lead to a full reduction of the $7b_2$ and $11a_1$ emission intensities. We link this remaining intensity to scattering in symmetry broken configurations that can arise from fluctuations in the chemical environment. The degree of solute−solvent interaction induced symmetry breaking in an aqueous environment is assessed through a comparison between the experimental RIXS data and results of molecular dynamics simulations. Furthermore, we show that the Jahn−Teller effect, splitting the degenerate nitrogen 1s core-excited states, induces a large antisymmetric distortion in the RIXS intermediate state which suppresses the partial cancellation of transition dipole moments for the lone-pair emission. Using a vibronic Kramers−Heisenberg formalism we are able to capture the drastic dependence on the excitation energy observed in the experimental spectra and predict details on the vibrational substructure of individual electronic transitions that could be assessed in future high-resolution RIXS measurements. We directly quantify the degree of core-induced symmetry breaking within the scattering process as well as the structural distortions induced by intermolecular interactions in solution. These findings address an underexplored aspect of chemical RIXS studies and have direct impact on the interpretation of spectra of symmetric molecules in solution. We demonstrate that detuning dependent RIXS spectra allow to disentangle core-excited Jahn−Teller induced- from solvent-induced distortions. We therefore expect even stronger RIXS signatures for molecules of higher symmetry and could foresee drastic differences for isomeric systems. In this context, also the role of more weakly interacting nonpolar and aprotic solvents inducing geometry fluctuations through instantaneous solvent polarization requires investigation.

## EXPERIMENTAL DETAILS

The sample was prepared as a 0.3 M aqueous solution of pyrimidine at pH 12.4 to guarantee a deprotonation of both N atoms of the system. The pH was adjusted using sodium hydroxide. The RIXS measurements were performed in the liquid flexRIXS experiment at the U49−2_PGM-1 beamline of the synchrotron BESSY II.[35] Complementary measurements have been performed at the EDAX experiment at the UE49_SGM beamline. The sample was injected into the experimental vacuum chamber as a liquid jet with a 20 $\mu$m diameter and excited with horizontally polarized radiation with a photon energy at the nitrogen 1s absorption edge and 250 meV bandwidth. The emitted radiation was detected in a 90° scattering geometry using a modified Scienta XES 350 spectrometer.

## ASSOCIATED CONTENT

### Supporting Information

The Supporting Information is available free of charge at https://pubs.acs.org/doi/10.1021/acs.jpclett.1c01865.

Complete description of theoretical simulations and mathematical formulation of the symmetry breaking problem (PDF)

## AUTHOR INFORMATION


### Corresponding Authors

**Sebastian Eckert** − *Institute for Methods and Instrumentation for Synchrotron Radiation Research, Helmholtz-Zentrum Berlin für Materialien und Energie GmbH, 12489 Berlin, Germany*; orcid.org/0000-0002-1310-0735; Email: sebastian.eckert@helmholtz-berlin.de

**Vinícius Vaz da Cruz** − *Institute for Methods and Instrumentation for Synchrotron Radiation Research, Helmholtz-Zentrum Berlin für Materialien und Energie GmbH, 12489 Berlin, Germany*; Email: vinicius.vaz_da_cruz@helmholtz-berlin.de

### Authors

**Miguel Ochmann** − *Center for Free-Electron Laser Science, Institute for Nanostructure and Solid State Physics, University of Hamburg, 22761 Hamburg, Germany*

**Inga von Ahnen** − *Center for Free-Electron Laser Science, Institute for Nanostructure and Solid State Physics, University of Hamburg, 22761 Hamburg, Germany*

**Alexander Föhlisch** − *Institut für Physik und Astronomie, Universität Potsdam, 14476 Potsdam, Germany; Institute for Methods and Instrumentation for Synchrotron Radiation Research, Helmholtz-Zentrum Berlin für Materialien und Energie GmbH, 12489 Berlin, Germany*

**Nils Huse** − *Center for Free-Electron Laser Science, Institute for Nanostructure and Solid State Physics, University of Hamburg, 22761 Hamburg, Germany*; orcid.org/0000-0002-3281-7600

Complete contact information is available at: https://pubs.acs.org/10.1021/acs.jpclett.1c01865


### Notes

The authors declare no competing financial interest.

## ACKNOWLEDGMENTS

We thank the Helmholtz-Zentrum Berlin for the allocation of synchrotron radiation beamtime. A.F. acknowledges funding from the ERC-ADG-2014 Advanced Investigator Grant No. 669531 EDAX under the Horizon 2020 EU Framework, Programme for Research and Innovation. We thank Markus Hantschmann for assistance during the measurements. N.H. and M.O. acknowledge funding by the Max Planck Society, the City of Hamburg and the collaborative research center SFB 925 of the German Science Foundation (DFG), project A4.

## REFERENCES


(1) Jahn, H. A.; Teller, E. Stability of Polyatomic Molecules in Degenerate Electronic States - I — Orbital degeneracy. *Proc. R. Soc. London A. Math. Phys. Sci.* **1937**, *161*, 220−235.

(2) Domcke, W.; Cederbaum, L. Vibronic Coupling and Symmetry Breaking in Core Electron Ionization. *Chem. Phys.* **1977**, *25*, 189−196.

(3) Gel'mukhanov, F.; Ågren, H. Resonant Inelastic X-ray Scattering with Symmetry-Selective Excitation. *Phys. Rev. A: At., Mol., Opt. Phys.* **1994**, *49*, 4378−4389.

(4) Cederbaum, L. S. Symmetry Breaking and Localization in Resonant Photon Emission. *J. Chem. Phys.* **1995**, *103*, 562−567.

(5) Skytt, P.; Glans, P.; Guo, J.-H.; Gunnelin, K.; Såthe, C.; Nordgren, J.; Gel'mukhanov, F.; Cesar, A.; Ågren, H. Quenching of Symmetry Breaking in Resonant Inelastic X-Ray Scattering by Detuned Excitation. *Phys. Rev. Lett.* **1996**, *77*, 5035−5038.

(6) Gel'mukhanov, F.; Ågren, H. Resonant X-ray Raman Scattering. *Phys. Rep.* **1999**, *312*, 87−330.

(7) Gel'mukhanov, F.; Sałek, P.; Privalov, T.; Ågren, H. Duration of X-ray Raman Scattering. *Phys. Rev. A: At., Mol., Opt. Phys.* **1999**, *59*, 380−389.

(8) Maganas, D.; Kristiansen, P.; Duda, L.-C.; Knop-Gericke, A.; DeBeer, S.; Schlögl, R.; Neese, F. Combined Experimental and Ab Initio Multireference Configuration Interaction Study of the Resonant Inelastic X-ray Scattering Spectrum of $CO_2$. *J. Phys. Chem. C* **2014**, *118*, 20163−20175.

(9) Harada, Y.; Tokushima, T.; Takata, Y.; Takeuchi, T.; Kitajima, Y.; Tanaka, S.; Kayanuma, Y.; Shin, S. Dynamical Symmetry Breaking under Core Excitation in Graphite: Polarization Correlation in Soft X-Ray Recombination Emission. *Phys. Rev. Lett.* **2004**, *93*, 017401.

(10) Hennies, F.; Polyutov, S.; Minkov, I.; Pietzsch, A.; Nagasono, M.; Gel'mukhanov, F.; Triguero, L.; Piancastelli, M.-N.; Wurth, W.; Ågren, H.; et al. Nonadiabatic Effects in Resonant Inelastic X-Ray Scattering. *Phys. Rev. Lett.* **2005**, *95*, 163002.

(11) Eckert, S.; Norell, J.; Miedema, P. S.; Beye, M.; Fondell, M.; Quevedo, W.; Kennedy, B.; Hantschmann, M.; Pietzsch, A.; Van Kuiken, B. E.; et al. Ultrafast Independent N-H and N-C Bond Deformation Investigated with Resonant Inelastic X-Ray Scattering. *Angew. Chem., Int. Ed.* **2017**, *56*, 6088−6092.

(12) Jeyachandran, Y. L.; Meyer, F.; Nagarajan, S.; Benkert, A.; Bär, M.; Blum, M.; Yang, W.; Reinert, F.; Heske, C.; Weinhardt, L.; et al. Ion-Solvation-Induced Molecular Reorganization in Liquid Water Probed by Resonant Inelastic Soft X-ray Scattering. *J. Phys. Chem. Lett.* **2014**, *5*, 4143−4148.

(13) Savchenko, V.; Brumboiu, I. E.; Kimberg, V.; Odelius, M.; Krasnov, P.; Liu, J.-C.; Rubensson, J.-E.; Björneholm, O.; Såthe, C.; Gråsjö, J.; et al. Vibrational Resonant Inelastic X-ray Scattering in Liquid Acetic Acid: a Ruler for Molecular Chain Lengths. *Sci. Rep.* **2021**, *11*, 4098.

(14) Wernet, P.; Kunnus, K.; Schreck, S.; Quevedo, W.; Kurian, R.; Techert, S.; de Groot, F. M. F.; Odelius, M.; Föhlisch, A. Dissecting Local Atomic and Intermolecular Interactions of Transition-Metal Ions in Solution with Selective X-ray Spectroscopy. *J. Phys. Chem. Lett.* **2012**, *3*, 3448−3453.

(15) Kunnus, K.; Zhang, W.; Delcey, M. G.; Pinjari, R. V.; Miedema, P. S.; Schreck, S.; Quevedo, W.; Schröder, H.; Föhlisch, A.; Gaffney, K. J.; et al. Viewing the Valence Electronic Structure of Ferric and Ferrous Hexacyanide in Solution from the Fe and Cyanide Perspectives. *J. Phys. Chem. B* **2016**, *120*, 7182−7194.

(16) Jay, R. M.; Eckert, S.; Van Kuiken, B. E.; Ochmann, M.; Hantschmann, M.; Cordones, A. A.; Cho, H.; Hong, K.; Ma, R.; Lee, J. H.; et al. Following Metal-to-Ligand Charge-Transfer Dynamics with Ligand and Spin Specificity Using Femtosecond Resonant Inelastic X-ray Scattering at the Nitrogen K-Edge. *J. Phys. Chem. Lett.* **2021**, *12*, 6676−6683.

(17) Vaz da Cruz, V.; Gel'mukhanov, F.; Eckert, S.; Iannuzzi, M.; Ertan, E.; Pietzsch, A.; Couto, R. C.; Niskanen, J.; Fondell, M.; Dantz, M.; et al. Probing Hydrogen Bond Strength in Liquid Water by Resonant Inelastic X-ray Scattering. *Nat. Commun.* **2019**, *10*, 1013.

(18) Weinhardt, L.; Benkert, A.; Meyer, F.; Blum, M.; Hauschild, D.; Wilks, R. G.; Bär, M.; Yang, W.; Zharnikov, M.; Reinert, F.; et al. Local Electronic Structure of the Peptide Bond Probed by Resonant Inelastic Soft X-ray Scattering. *Phys. Chem. Chem. Phys.* **2019**, *21*, 13207−13214.

(19) Eckert, S.; Niskanen, J.; Jay, R. M.; Miedema, P. S.; Fondell, M.; Kennedy, B.; Quevedo, W.; Iannuzzi, M.; Föhlisch, A. Valence Orbitals and Local Bond Dynamics Around N Atoms of Histidine Under X-ray Irradiation. *Phys. Chem. Chem. Phys.* **2017**, *19*, 32091−32098.

(20) Meyer, F.; Blum, M.; Benkert, A.; Hauschild, D.; Jeyachandran, Y. L.; Wilks, R. G.; Yang, W.; Bär, M.; Reinert, F.; Heske, C.; et al. Site-specific Electronic Structure of Imidazole and Imidazolium in Aqueous Solutions. *Phys. Chem. Chem. Phys.* **2018**, *20*, 8302−8310.

(21) Jay, R. M.; Norell, J.; Eckert, S.; Hantschmann, M.; Beye, M.; Kennedy, B.; Quevedo, W.; Schlotter, W. F.; Dakovski, G. L.; Minitti, M. P.; et al. Disentangling Transient Charge Density and Metal−Ligand Covalency in Photoexcited Ferricyanide with Femtosecond Resonant Inelastic Soft X-ray Scattering. *J. Phys. Chem. Lett.* **2018**, *9*, 3538−3543.

(22) Temperton, R. H.; Skowron, S. T.; Handrup, K.; Gibson, A. J.; Nicolaou, A.; Jaouen, N.; Besley, E.; O'Shea, J. N. Resonant Inelastic X-ray Scattering of a Ru Photosensitizer: Insights from Individual Ligands to the Electronic Structure of the Complete Molecule. *J. Chem. Phys.* **2019**, *151*, 074701.

(23) Melandri, S.; Sanz, M. E.; Caminati, W.; Favero, P. G.; Kisiel, Z. The Hydrogen Bond between Water and Aromatic Bases of Biological Interest: An Experimental and Theoretical Study of the 1:1 Complex of Pyrimidine with Water. *J. Am. Chem. Soc.* **1998**, *120*, 11504−11509.

(24) Schlücker, S.; Koster, J.; Singh, R. K.; Asthana, B. P. Hydrogen-Bonding between Pyrimidine and Water: A Vibrational Spectroscopic Analysis. *J. Phys. Chem. A* **2007**, *111*, 5185−5191.

(25) Manzoni, V.; Lyra, M. L.; Gester, R. M.; Coutinho, K.; Canuto, S. Study of the Optical and Magnetic Properties of Pyrimidine in Water Combining PCM and QM/MM Methodologies. *Phys. Chem. Chem. Phys.* **2010**, *12*, 14023−14033.

(26) Howard, A. A.; Tschumper, G. S.; Hammer, N. I. Effects of Hydrogen Bonding on Vibrational Normal Modes of Pyrimidine. *J. Phys. Chem. A* **2010**, *114*, 6803−6810.

(27) Vaz da Cruz, V.; Eckert, S.; Föhlisch, A. TD-DFT Simulations of K-edge Resonant Inelastic X-ray Scattering Within the Restricted Subspace Approximation. *Phys. Chem. Chem. Phys.* **2021**, *23*, 1835−1848.

(28) Vaz da Cruz, V.; Ignatova, N.; Couto, R. C.; Fedotov, D. A.; Rehn, D. R.; Savchenko, V.; Norman, P.; Ågren, H.; Polyutov, S.; Niskanen, J.; et al. Nuclear Dynamics in Resonant Inelastic X-ray Scattering and X-ray Absorption of Methanol. *J. Chem. Phys.* **2019**, *150*, 234301.

(29) Cacelli, I.; Ferretti, A.; Prampolini, G. Perturbative Multi-reference Configuration Interaction (CI-MRPT2) Calculations in a Focused Dynamical Approach: A Computational Study of Solvato-chromism in Pyrimidine. *J. Phys. Chem. A* **2015**, *119*, 5250−5259.

(30) Nijegorodov, N. I.; Downey, W. S. The Influence of Planarity and Rigidity on the Absorption and Fluorescence Parameters and Intersystem Crossing Rate Constant in Aromatic Molecules. *J. Phys. Chem.* **1994**, *98*, 5639−5643.

(31) Eckert, S.; Miedema, P.; Quevedo, W.; O'Cinneide, B.; Fondell, M.; Beye, M.; Pietzsch, A.; Ross, M.; Khalil, M.; Föhlisch, A. Molecular Structures and Protonation State of 2-Mercaptopyridine in Aqueous Solution. *Chem. Phys. Lett.* **2016**, *647*, 103−106.

(32) Büchner, R.; Fondell, M.; Mascarenhas, E. J.; Pietzsch, A.; Vaz da Cruz, V.; Föhlisch, A. How Hydrogen Bonding Amplifies Isomeric Differences in Pyridones toward Strong Changes in Acidity and Tautomerism. *J. Phys. Chem. B* **2021**, *125*, 2372−2379.

(33) Lord, R.; Marston, A.; Miller, F. A. Infra-red and Raman spectra ot the Diazines. *Spectrochim. Acta* **1957**, *9*, 113−125.

(34) Eckert, S.; Vaz da Cruz, V.; Gel'mukhanov, F.; Ertan, E.; Ignatova, N.; Polyutov, S.; Couto, R. C.; Fondell, M.; Dantz, M.; Kennedy, B.; et al. One-dimensional Cuts Through Multidimensional




https://doi.org/10.1021/acs.jpclett.1c01865
J. Phys. Chem. Lett. 2021, 12, 8637−8643

Potential-Energy Surfaces by Tunable X Rays. *Phys. Rev. A: At., Mol., Opt. Phys.* **2018**, *97*, 053410.
(35) Kunnus, K.; Rajkovic, I.; Schreck, S.; Quevedo, W.; Eckert, S.; Beye, M.; Suljoti, E.; Weniger, C.; Kalus, C.; Grübel, S.; et al. A Setup for Resonant Inelastic Soft X-ray Scattering On Liquids at Free Electron Laser Light Sources. *Rev. Sci. Instrum.* **2012**, *83*, 123109.



https://doi.org/10.1021/acs.jpclett.1c01865
*J. Phys. Chem. Lett.* 2021, 12, 8637−8643